Aalborg Universitet

Novel Space Vector Pulsewidth Modulation Strategies for Single-Phase Three-Level NPC Impedance-Source Inverters

Shults, T. E.; Husev, O.; Blaabjerg, F.; Roncero-Clemente, C.; Romero-Cadaval, E.; Vinnikov, D.

Novel Space Vector Pulse Width Modulation Strategies for Single-Phase Three-Level NPC Impedance-Source Inverters

Tatiana Shults, Oleksandr Husev, *Member, IEEE*, Frede Blaabjerg, *Fellow, IEEE*, Carlos Roncero-Clemente, *Member, IEEE*, Enrique Romero-Cadaval, *Senior Member, IEEE*, Dmitri Vinnikov, *Senior Member, IEEE*

Abstract— **This paper presents new Space Vector Pulse-Width Modulation (SVPWM) strategies for a single-phase three-level buck-boost Neutral Point Clamped (NPC) inverter coupled with Impedance-Source (IS) networks. These strategies can be implemented for systems with any IS networks with neutral point. The case study system is based on the quasi-Z-source inverter with continuous input current. To demonstrate an improved performance, the strategies are compared with a traditional pulse-width modulation strategy. The advantages lie in reduced switching number, without output voltage quality distortion. The simulation and experimental results confirm the theoretical predictions.**

I. INTRODUCTION

Present technologies and innovations have led to the expansion of Photovoltaic (PV) energy generation systems worldwide [1]-[4]. PV energy sources are characterized by a wide output voltage and power variation. The solar irradiation level changes significantly during the day and gives a variable output power. Also, the shading or high operating temperature of the PV module leads to a significant out-voltage drop. Therefore, the converter for a PV system should have a wide input voltage and output load regulation range.

To extend the input voltage regulation range, solutions based on Impedance-Source (IS) networks have been proposed [5]-[11]. They have a buck mode, a boost mode and do not suffer from the Shoot-Through (ST) [5] states compare to the conventional grid-connected inverters.

Tatina Shults is with the Power Electronics Institute of Novosibirsk State Technical University 20, Prospekt K. Marksa, Novosibirsk, 630073, Russia

Oleksandr Husev and Dmitri Vinnikov are with the Department of Electrical Power Engineering and Mechatronics, Tallinn University of Technology, Ehitajate str. 5, 19086 Tallinn, Estonia. Oleksandr Husev is also with the Department of Biomedical Radioelectronics Apparatus and Systems, Chernihiv National University of Technology, Shevchenko str. 95, 14027 Chernihiv, Ukraine (e-mail: oleksandr.husev@ieee.org).

Frede Blaabjerg is with the Institute of Energy Technology, Aalborg University, Pontoppidanstræde, str. 101, 9220 Aalborg, Denmark (e-mail: fbl@et.aau.dk).

Carlos Roncero-Clemente and Enrique Romero-Cadaval are with the School of Industrial Engineering, University of Extremadura, Avda. Elvas s/n, 06006, Badajoz, Spain (e-mail: croncero@peandes.net, ercadaval@ieee.org).

At the same time, inverters used for PV system integration to the grid can be based on two-level or multilevel topologies. Multilevel inverters are preferable solutions not only for medium-voltage but also for low-voltage applications. One of the most important benefits of the multilevel inverter is reduced voltage stress on the semiconductors. At the same time, the increased number of the output voltage levels leads to an output voltage quality improvement. The Three-Level (3L) Neutral Point Clamped (NPC) inverter is one of the most popular solutions among the multilevel topologies [12]-[18]. In case of full-bridge utilization it gives five-level output voltage.

The latest research [19]-[21] show that any IS networks are feasible for low power application with a wide range input voltage regulation. In most applications, low power facilities are associated with single-phase systems. The latest research [19]-[21] show that any IS networks are feasible for low power application with a wide range input voltage regulation. In most applications, low power facilities are associated with single-phase systems.

Low power applications make such topologies feasible by means of a very high switching frequency that, in turn, reduces the size and weight of the passive components. Switching losses can be reduced by means of novel wide bandgap semiconductors and also different modulation techniques.

There are many well-known Pulse-Width Modulation (PWM) techniques that can be applied for IS based converters [22]-[31]. Space Vector PWM (SVPWM) is mostly applied to three-phase systems [32]-[39]. It can be applied for IS based converters as well [40]-[43].

At the same time, several papers report that SVPWM is suitable for conventional single-phase systems [44]-[47]. Additionally, this technique is effective for use with a voltage unbalancing problem [44]. This technique is proposed only for conventional single-phase three-level inverters. Focus in this work is on the development of a SVPWM for the single-phase 3L NPC buck-boost inverter coupled with any IS network. SVPWM makes the neutral point balancing flexible, improves the output voltage quality, and reduces also the switching losses.

II. EXISTING SVPWM TECHNIQUES FOR SINGLE-PHASE THREE-LEVEL INVERTER

The 3L NPC buck-boost inverter coupled with IS (quasi-Z-source) network is shown in Fig. 1, where points -1, 0, 1, A, and B are denoted. The 3L quasi-Z-Source NPC inverter is selected as a case study solution [15].
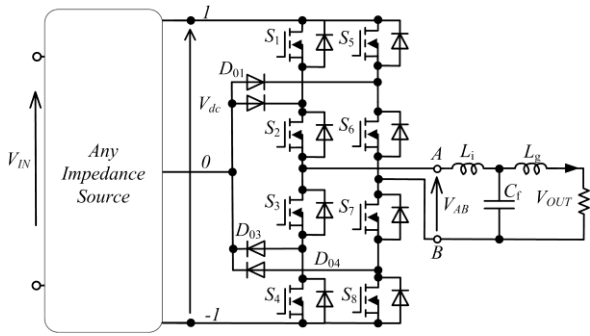
Fig. 1. Single-Phase 3L NPC inverter coupled with IS networks.

Nine switching states are possible for a conventional 3L NPC converter: (-1,-1), (0,0), (1,1), (-1,0), (0,1), (1,-1), (0,-1), (-1,1), and (1,-1), that are illustrated in Table I. Where 1 is denoted as conducting switches S_1-S_8.

TABLE I. SWITCHING STATES FOR A SINGLE-PHASE NPC

State	S_1	S_2	S_3	S_4	S_5	S_6	S_7	S_8	Voltage level V_{AB}	Vectors (Fig. 2a)	Vectors (Fig. 2b)
-1,-1	0	0	1	1	0	0	1	1	0		
0,0	0	1	1	0	0	1	1	0	0	V_0	V_0
1,1	1	1	0	0	1	1	0	0	0		
1,0	1	1	0	0	0	1	1	0	$V_{dc}/2$	V_4	V_1
0,-1	0	1	1	0	0	0	1	1	$V_{dc}/2$	V_2	
1,-1	1	1	0	0	0	0	1	1	V_{dc}	V_3	V_2
0,1	0	0	1	1	1	1	0	0	$- V_{dc}/2$	V_1	V_3
-1,0	0	0	1	1	0	1	1	0	$- V_{dc}/2$	V_5	
-1,1	0	0	1	1	1	1	0	0	$- V_{dc}$	V_6	V_4

Using these switching states, two space voltage vector diagrams can be shown [45] for a single-phase 3L NPC inverter (Fig. 2).

Fig. 2a represents a reference vector V^* synthesized by six non-zero voltage vectors V_1-V_6 and one zero voltage vector V_0. In each of the six sectors (*I-VI*) three closer located vectors are used V_j, V_{j+1} and V_0, for synthesizing the reference vector V^*, where j is a vector number. In sector *VI*, the reference vector V^* is synthesized by V_1, V_6 and V_0. The use of V_0 is necessary in order to provide the modulation index in a range of $0 \leq M \leq 1$.

A weighting coefficient τ_{ij} will be used for the following analysis, where i is the sector number. The weighting coefficient τ_{ij} is the relative duration of the vector V_j during the switching period in sector i. For any sector in Fig. 2a, the weighting coefficients τ can be defined from:

$$\begin{cases} \tau_0 = 1 - \dfrac{M}{\sqrt{3}} \cdot \left(\cos(\vartheta) + \dfrac{1}{\sqrt{3}} \sin(\vartheta) \right) \\[2mm] \tau_{i,j} = \dfrac{M}{\sqrt{3}} \cdot \left(\cos(\vartheta) - \dfrac{1}{\sqrt{3}} \sin(\vartheta) \right) \\[2mm] \tau_{i,(j+1)} = \dfrac{2}{3} \cdot M \cdot \sin(\vartheta) \\[2mm] \tau_{i,j} + \tau_{i,(j+1)} + \tau_0 = 1, \tau_{i,j} = \dfrac{T_{i,j}}{T}, 0° < \vartheta \leq 60° \end{cases} \quad (1)$$

where $T_{i,j}$ is the time interval of the space vector application, T is the switching period.

In the SVPWM shown in Fig. 2b, the reference vector V^* is synthesized by four non-zero voltage vectors V_1-V_4

and one zero voltage vector V_0. In each of the eight sectors (*I-VIII*) for synthesizing the reference vector V^*, two closer located vectors are used. For example, V_1 and V_0 are used in sector *I*, and V_4 and V_3 in sector *VII*. The weighting coefficients for this approach are given in Table II, where phase ϑ is varying in a range $0° < \vartheta \leq 360°$ and S is the number of the sectors.
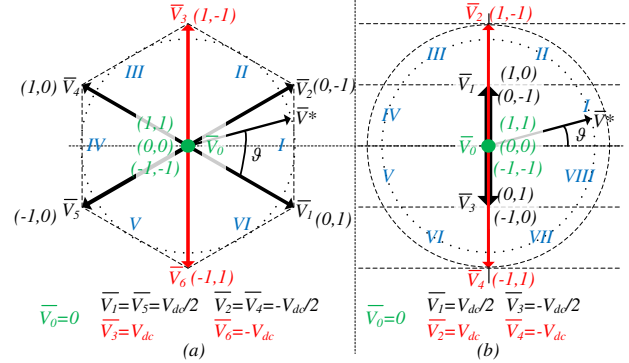

Fig. 2. Space voltage vector diagrams for a single-phase 3L NPC inverter derived by different set of vectors (a and b).

TABLE II. WEIGHTING COEFFICIENTS FOR SVPWM IN DIFFERENT SECTORS (FIG. 2B)

Sector	Weighting coefficients (τ_{ij})
I, IV	$\begin{cases} \tau_{1,0} = \tau_{4,0} = 1 - 2M \sin(\vartheta) \\ \tau_{1,1} = \tau_{4,1} = 2M \sin(\vartheta) \end{cases}$
II, III	$\begin{cases} \tau_{2,1} = \tau_{3,1} = 2 - 2M \sin(\vartheta) \\ \tau_{2,2} = \tau_{3,2} = 2M \sin(\vartheta) - 1 \end{cases}$
V, VIII	$\begin{cases} \tau_{5,0} = \tau_{8,0} = 1 + 2M \sin(\vartheta) \\ \tau_{5,3} = \tau_{8,3} = -2M \sin(\vartheta) \end{cases}$
VI, VII	$\begin{cases} \tau_{6,3} = \tau_{7,3} = 2 + 2M \sin(\vartheta) \\ \tau_{6,4} = \tau_{7,4} = -1 - 2M \sin(\vartheta) \end{cases}$

In a general case, the weighting coefficients for any SVPWM are calculated according to the principle proposed in [44]. The SVPWM shown in Fig. 2b has several key advantages over the SVPWM shown in Fig. 2a. First of all, it has 15% larger fundamental harmonic component. Also, the calculation of the weighting coefficients is much easier. Therefore, the SVPWM is shown in Fig. 2b will be considered like a basic solution.

III. SVPWM FOR SINGLE-PHASE IS-BASED INVERTER

Fig. 3 shows a proposed space vector diagram for an IS-based Single-Phase 3L NPC inverter along with an example of the switching states distribution in each sector. The main goal of this approach lies in the generation of the optimal switching sequence in terms of minimum switching losses providing the output sinusoidal voltage. At the same time, it should be noted that only equally distributed ST generation is considered. Maximum boost control [22] may evoke oscillation in the IS network and is not feasible for practical implementation. This phenomenon has been shown and discussed in [48].
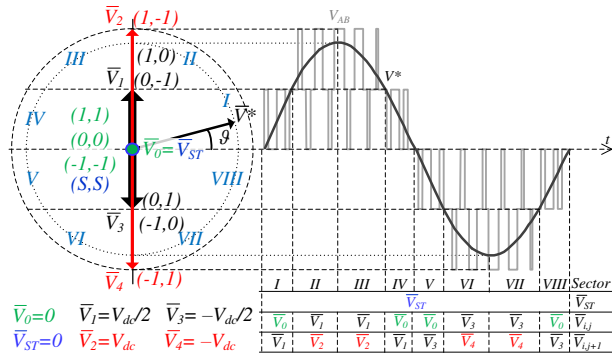
Fig. 3. Space voltage vector diagram for proposed SVPW for single-phase 3L NPC IS inverter.

The vector diagram is divided into eight sectors. It is different by additional ST vector V_{ST}, which is in a response for ST state generation. However, here in each sector, three weighting coefficients must be defined: two for general (closer located) vectors and one for the vector V_{ST}. The vector V_{ST} is used in each sector in order to achieve equally distributed ST generation. The weighting coefficient of V_{ST} is equal to ST duty cycle D_{ST}, determined by capacitor voltage regulator. Taking into account equally distributed ST states (τ_{ST}=const) the weighting coefficients are defined as:

$$
\begin{cases}
\tau_{ST} = D_S = T_{ST}/T = const, M \leq 1 \\
\tau_{ST} + \tau_{i,j} + \tau_{i,(j+1)} = 1 \\
\tau_{i,j} = \dfrac{(1-\tau_{ST}) \cdot \vec{V}_{j+1} - \vec{V}^*}{\vec{V}_{j+1} - \vec{V}_j} \\
\tau_{i,(j+1)} = \dfrac{(1-\tau_{ST}) \cdot \vec{V}_j - \vec{V}^*}{\vec{V}_j - \vec{V}_{j+1}}
\end{cases}
\qquad (2)
$$

where V_j, V_{j+1} are the space vectors used in sector i and $V^*=(1-\tau_{ST}) \cdot M \cdot V_{dc} \sin(\vartheta)$ is the reference vector.

For example, in the sector VII, the output voltage is generated by vectors $\vec{V}_j = \vec{V}_3 = -V_{dc}/2$ and $\vec{V}_{j+1} = \vec{V}_4 = -V_{dc}$. The weighting coefficients are expressed from (2) as:

$$
\begin{cases}
\tau_{i,j+1} = \tau_{7,4} = \dfrac{(1-\tau_{ST})(\frac{-V_{dc}}{2}) - (1-\tau_{ST})M \cdot V_{dc} \sin \vartheta}{-\frac{V_{dc}}{2} - (-V_{dc})} \\
\tau_{i,j} = \tau_{7,3} = \dfrac{(1-\tau_{ST})(-V_{dc}) - (1-\tau_{ST})M \cdot V_{dc} \sin \vartheta}{-V_{dc} - (-\frac{V_{dc}}{2})}
\end{cases}
, (3)
$$

$$
\begin{cases}
\tau_{7,4} = \tau_{ST} - 1 - 2 \cdot V_Y^* \\
\tau_{7,3} = (1-\tau_{ST}) \cdot 2 + 2 \cdot V_Y^*
\end{cases},
\qquad (4)
$$

$$
V_Y^* = (1-\tau_{ST}) \cdot M \cdot \sin \vartheta. \qquad (5)
$$

Here (5) V^*_Y is y axis projection of V^* in relative units. The calculated weighting coefficients for all sectors are shown in Table III. The vector V^* position and sector boundaries are detected by calculating the rotation angle ϑ value.

One of the very important issues during generation of the sequence of the vector is balancing of the energy utilization from capacitors. It consists in the equal charging and discharging of the different capacitors of IS network. Fig. 4 shows two equivalent switching states of the vector V_1 which generates the voltage equal to $V_{dc}/2$.

In the first case (Fig. 4a) the charging current of capacitor C_2 ($i_{C2}=i_{IN}$) is larger than the charging current of capacitor C_3 ($i_{C3}=i_{IN} - i_{dc}$) and vice-versa in the second case (Fig. 4b). The principle of the balancing consists in equal utilization of the equivalent circuits shown in Fig. 4 maintaining constant voltage across the capacitors.

(a)

(b)
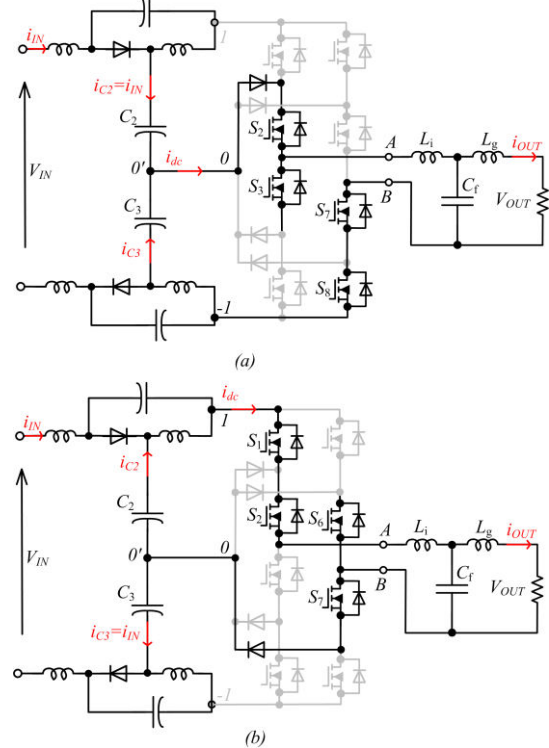
Fig. 4. Equivalent circuits of active states of the quasi-Z-Source NPC inverter.

TABLE III. WEIGHTING COEFFICIENTS OF SVPWM FOR IS INVERTER (FIG. 3)

Weighting coefficients (τ_{ij})	Sector boundaries	
$\begin{cases} \tau_{1,0} = \tau_{40,} = 1-\tau_{ST} - 2 \cdot V_Y^* \\ \tau_{1,1} = \tau_{4,1} = 2 \cdot V_Y^* \end{cases}$	$I : 0 \leq \vartheta < \arcsin\left(\dfrac{0.5}{M}\right)$	$IV : \pi - \arcsin\left(\dfrac{0.5}{M}\right) \leq \vartheta < \pi$
$\begin{cases} \tau_{2,1} = \tau_{3,1} = (1-\tau_{ST}) \cdot 2 - 2 \cdot V_Y^* \\ \tau_{2,2} = \tau_{3,2} = -(1-\tau_{ST}) + 2 \cdot V_Y^* \end{cases}$	$II : \arcsin\left(\dfrac{0.5}{M}\right) \leq \vartheta < \dfrac{\pi}{2}$	$III : \dfrac{\pi}{2} \leq \vartheta < \pi - \arcsin\left(\dfrac{0.5}{M}\right)$
$\begin{cases} \tau_{5,0} = \tau_{8,0} = 1-\tau_{ST} + 2 \cdot V_Y^* \\ \tau_{5,3} = \tau_{8,3} = -2 \cdot V_Y^* \end{cases}$	$V : \pi \leq \vartheta < \pi + \arcsin\left(\dfrac{0.5}{M}\right)$	$VIII : 2\pi - \arcsin\left(\dfrac{0.5}{M}\right) \leq \vartheta < 2\pi$
$\begin{cases} \tau_{6,3} = \tau_{7,3} = 2 \cdot (1-\tau_{ST}) + 2 \cdot V_Y^* \\ \tau_{6,4} = \tau_{7,4} = -(1-\tau_{ST}) - 2 \cdot V_Y^* \end{cases}$	$VI : \pi + \arcsin\left(\dfrac{0.5}{M}\right) \leq \vartheta < \dfrac{3\pi}{2}$	$VII : \dfrac{3\pi}{2} \leq \vartheta < 2\pi - \arcsin\left(\dfrac{0.5}{M}\right)$

Fig. 5. Switching states sequences in the proposed SVPWM single-phase IS inverter.

The switching states (SS) distribution is shown in Fig. 5. It can be noted that a switching state sequence of sectors III, IV and VII, VIII is the mirror image of sectors I, II and V, VI, respectively. Grey color means conducting semiconductor switches of the inverter. One of the direct criteria of the switching optimization is overall number of transistor commutation per switching cycle. In this case, the overall commutation number per switching cycle is 12. It should be noticed, than in case of dropping modulation index less than 0.5, the sectors II, III, VI and VII will not be involved in the output voltage vector generation. It can be seen from Fig. 3. At the same time, the number of transistor commutation per switching cycle remains the same. It is explained by fact that all sectors have equal commutation number per switching cycle (Fig. 5).

Summarizing above presented approach it includes calculation of the weighting coefficients of the vectors for each sector in order to provide sinusoidal waveform of the output voltage and select a proper switching sequence in order to provide constant voltage across capacitors along with minimum number of transistor switching.

IV. MODIFIED SVPWM FOR SINGLE-PHASE IS-BASED INVERTER

Incomplete ST states are mentioned in several papers concerning three-phase systems with impedance networks [29], [30]. The feature of this state consists of asymmetrical ST application to one out of two networks. At the same time the voltage applied to the output is not equal to zero. The equivalent circuit of the additional ST state (1,S) for 3L NPC quasi-Z-Source inverter is depicted in Fig. 6. It shows that only the lower part (IS2) of the quasi-Z-Source network corresponds to the ST state. Capacitor C_3 is discharging and C_2 is charging.

Fig. 6. Equivalent circuit of additional incomplete ST state (1,S) of the quasi-Z-Source NPC inverter.

Additional switching states of incomplete ST can be implemented in order to reduce number of switching. In total, there are four incomplete ST states: (1,S), (S,-1), (S,1) and (-1,S). S denotes an incomplete short circuit

when only three switches are opened in the inverter leg. Because of that switching period, both (1,S) and (S,-1) or (S,1) and (-1,S) states should be used during the switching period. Using only one incomplete ST switching state per switching period leads to a capacitor voltage unbalance. However, the voltage V_{AB} at an incomplete ST state is $V_{dc}/2$. These additional states give additional flexibility in the output voltage vector generation. The weighting coefficients and sector boundaries are shown in Table IV.

Fig. 7a shows a proposed space vector diagram for the modified SVPWM along with an example of the switching states distribution in each sector.

(a)

(b)

Fig. 7. Space voltage vector diagram for proposed modified SVPWM for single-phase 3L NPC IS inverter (a) along with switching states sequences (b).

The switching state sequences for the modified SVPWM are shown in Fig. 7b. Vectors V_{ST1} and V_1 are equal and co-directional, as well as V_{ST3} and V_3.

TABLE IV. WEIGHTING COEFFICIENTS OF MODIFIED SVPWM (FIG. 8)

Weighting coefficients (τ_{ij})	Sector boundaries	
$\begin{cases}\tau_{1,0}=\tau_{6,0}=1-\tau_{ST}-2\cdot V_Y^* \\ \tau_{1,1}=\tau_{6,1}=2\cdot V_Y^*\end{cases}$	$I:0\le\vartheta<\arcsin\left(\dfrac{0.5}{M}\right)$	$VI:\pi-\arcsin\left(\dfrac{0.5}{M}\right)\le\vartheta<\pi$
$\begin{cases}\tau_{2,0}=\tau_{5,0}=1-2\cdot V_Y^* \\ \tau_{2,1}=\tau_{5,1}=2\cdot V_Y^*-\tau_{ST}\end{cases}$	$II:\arcsin\left(\dfrac{0.5}{M}\right)\le\vartheta<\arcsin\left(\dfrac{0.5}{M\cdot(1-D_S)}\right)$	$V:\pi-\arcsin\left(\dfrac{0.5}{M\cdot(1-D_S)}\right)\le\vartheta<\pi-\arcsin\left(\dfrac{0.5}{M}\right)$
$\begin{cases}\tau_{3,1}=\tau_{4,1}=2-\tau_{ST}-2\cdot V_Y^* \\ \tau_{3,2}=\tau_{4,2}=-1+2\cdot V_Y^*\end{cases}$	$III:\arcsin\left(\dfrac{0.5}{M\cdot(1-D_S)}\right)\le\vartheta<\dfrac{\pi}{2}$	$IV:\dfrac{\pi}{2}\le\vartheta<\pi-\arcsin\left(\dfrac{0.5}{M\cdot(1-D_S)}\right)$
$\begin{cases}\tau_{7,0}=\tau_{12,0}=1-\tau_{ST}+2\cdot V_Y^* \\ \tau_{7,3}=\tau_{12,3}=-2\cdot V_Y^*\end{cases}$	$VII:\pi\le\vartheta<\pi+\arcsin\left(\dfrac{0.5}{M}\right)$	$XI:2\pi-\arcsin\left(\dfrac{0.5}{M}\right)\le\vartheta<2\pi$
$\begin{cases}\tau_{8,0}=\tau_{11,0}=1+2\cdot V_Y^* \\ \tau_{8,3}=\tau_{11,13}=-2\cdot V_Y^*-\tau_{ST}\end{cases}$	$VIII:\pi+\arcsin\left(\dfrac{0.5}{M}\right)\le\vartheta<\pi+\arcsin\left(\dfrac{0.5}{M\cdot(1-D_S)}\right)$	$XI:2\pi-\arcsin\left(\dfrac{0.5}{M\cdot(1-D_S)}\right)\le\vartheta<2\pi-\arcsin\left(\dfrac{0.5}{M}\right)$
$\begin{cases}\tau_{9,3}=\tau_{10,3}=2-\tau_{ST}+2\cdot V_Y^* \\ \tau_{9,4}=\tau_{10,4}=-1-2\cdot V_Y^*\end{cases}$	$IX:\pi+\arcsin\left(\dfrac{0.5}{M\cdot(1-D_S)}\right)\le\vartheta<\dfrac{3\pi}{2}$	$X:\dfrac{3\pi}{2}\le\vartheta<2\pi-\arcsin\left(\dfrac{0.5}{M\cdot(1-D_S)}\right)$

A switching state sequence of sectors IV-VII and X-XII is the mirror image of sectors I-III and VII-IX, respectively. The overall commutation number per switching period in sectors I, VI, VII, XII is 12. In all other sectors, the overall commutation number is 8. It can be seen that the commutation number in the modified SVPWM (Fig. 7*b*) is significantly reduced compared with SVPWM (Fig. 5). It corresponds to the 22% reduction of overall commutation number in case of $M·=1$.

In advance, the quality of the energy transfer from the source to the load is also improved.

If modulation index is lower, according to the Fig. 7*a*, the involvement of the sectors III, IV, IX and X will be reduced. The modulation index $M·=(1–D_{ST})·0.5$ is a borderline value when these sectors can be used. Since these sectors have only 8 transistors switching, the overall commutation number will be increased. At the same time, it should be mentioned, that in proper designed inverters, the modulation index lower than 0.5 is not expected. It corresponds to the poor dc-link voltage utilization.
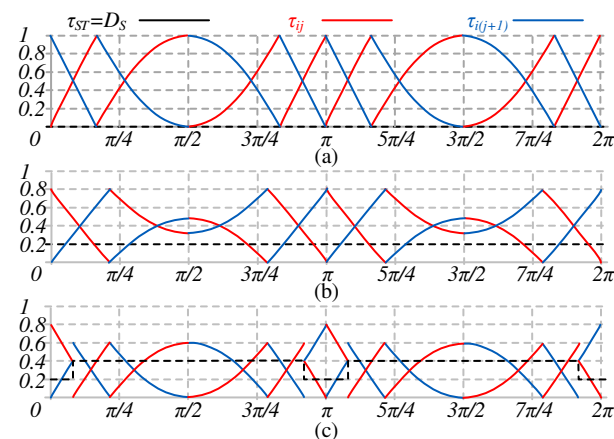

Fig. 8. Graphical representation of the weighting coefficients of:
(a) both SVPWM, M=1, D_{ST}=0; (b) the SVPWM, M=1, D_{ST}=0.2;
(c) the modified SVPWM, M=1, D_{ST}=0.2.

Finally, in graphical representation of the weighting coefficients is shown in Fig. 8. Fig. 8b and Fig. 8c illustrates the weighting coefficients for the case with ST duty cycle which is equal D_{ST}=0.2 and modulation index M=1 correspondingly. From Fig. 3, 7 and Table III, IV it can be seen that boundaries of the sectors strictly depends

on the amplitude of ST duty cycle. However if *M*=1 and D_{ST}=0 both SVPWMs have equal weighted coefficients representation like in Fig. 8a.

V. SIMULATION AND EXPERIMENTAL VERIFICATION

In order to verify the proposed approaches and to demonstrate the feasibility of the practical implementation, a comprehensive simulation and experimental study was performed. The main goal was to compare the proposed SVPWM for single-phase IS networks with existing modulation techniques. The value of components and parameters of the chosen topology are presented in Table IV [15], [16].

TABLE IV. COMPONENTS AND PARAMETERS OF 3L NPC QUASI-Z-SOURCE INVERTER USED FOR EXPERIMENTS

Input dc voltage V_{IN}	240-450 V
Output ac RMS voltage V_{OUT}	230 V
Nominal output power	1 kW
Capacitance value of the capacitors C_1 and C_4	1 mF
Capacitance value of the capacitors C_2 and C_3	0.4 mF
Inductance value of the inductors $L_1... L_4$	240 µH
Inverter side inductor filter L_I	0.44 mH
Output side inductor filter L_g	0.2 mH
Capacitor filter C_f	0.47 µF
Switching frequency f	120 - 240kHz
Control Unit (FPGA)	Cyclone IV EP4CE6E22C8
Control Unit (MC)	STM32F417ZET
Transistors Driver Chip	ACPL-H312
Transistors $S_1... S_8$	IPW65R041CFD
quasi-Z-Source and NPC diodes $D_1... D_6$	C3D10065A SiC Shottky

Fig. 9 shows the experimental setup. It consists of the inverter PCB board, a quasi-Z-Source board with external quasi-Z-Source inductors and output filters. The values of the passive components are shown in Table IV. Also, the control board is shown in Fig. 9. Table IV shows the values of passive elements along with types of selected semiconductors. It should be underlined that conventional Si MOSFET transistors from Infinion are selected. They belong to the family with very fast body diode and are adopted for inverter application. At the same time SiC diodes are selected as clamping diodes and diodes for

quasi-Z-source network. Any other types of diodes are not suitable for high switching frequency in IS based converters.
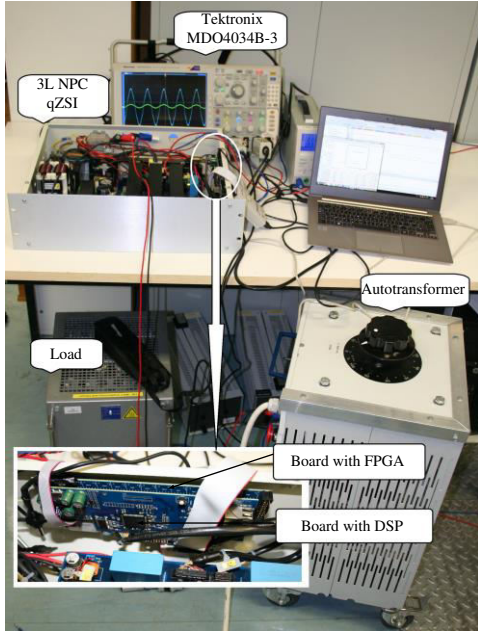

Fig. 9. Photo of the experimental setup along with the control board.

All the measurements were made by the digital oscilloscope Tektronix MDO4034B-3, current probes Tektronix TCP0150, and voltage probes Tektronix TPA-BNC. Fig. 9 shows a zoomed picture of the control board. It was specially designed for this application. The control system consists of two boards based on a combination of the low cost Field-Programmable Gate Array (FPGA) and Microcontroller (MC) with Floating-point Unit (FPU). The bottom side board has a low cost FPGA from Altera Cyclone IV EP4CE6E22C8. The upper side board has MC STM32F417ZET correspondingly. Each of these parts can work independently and communicate through Serial Peripheral Interface (SPI). Such combination provides an effective performance of any complex control.

Fig. 10 shows the diagram of the calculation sequence of the SVPWM techniques. First of all it can be seen that

calculation is distributed between MC and FPGA. The reference sinusoidal voltage V_{REF} is the input signal for MC. This signal is derived from another block that is not topic of discussion of this paper. The ST duty cycle D_S is derived from other control unit as well.
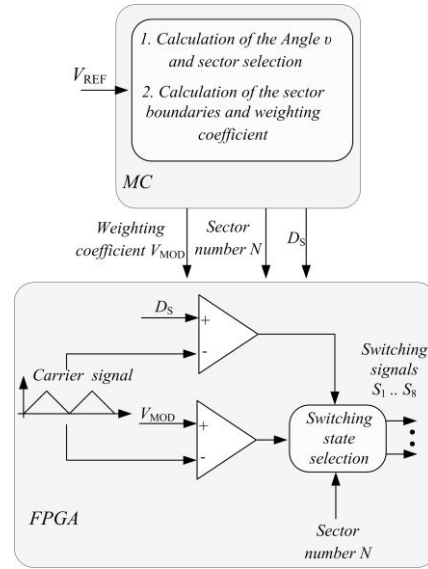

Fig. 10. Diagram of the calculation sequence of the SVPWM.

According to the phase and amplitude of the reference sinusoidal voltage MC defines the sector number along with weighting coefficient of the vectors. The FPGA is a suitable tool to realize a very high PWM switching frequency. The switching state selection that is realized in the FPGA requires no powerful computing resources. FPGA based on received weighting coefficient and sector number defines the switching states of transistors. It should be noted that final switching frequency can be much higher than frequency of data exchange between MC and FPGA. The switching frequency is defined by carrier signal in FPGA.
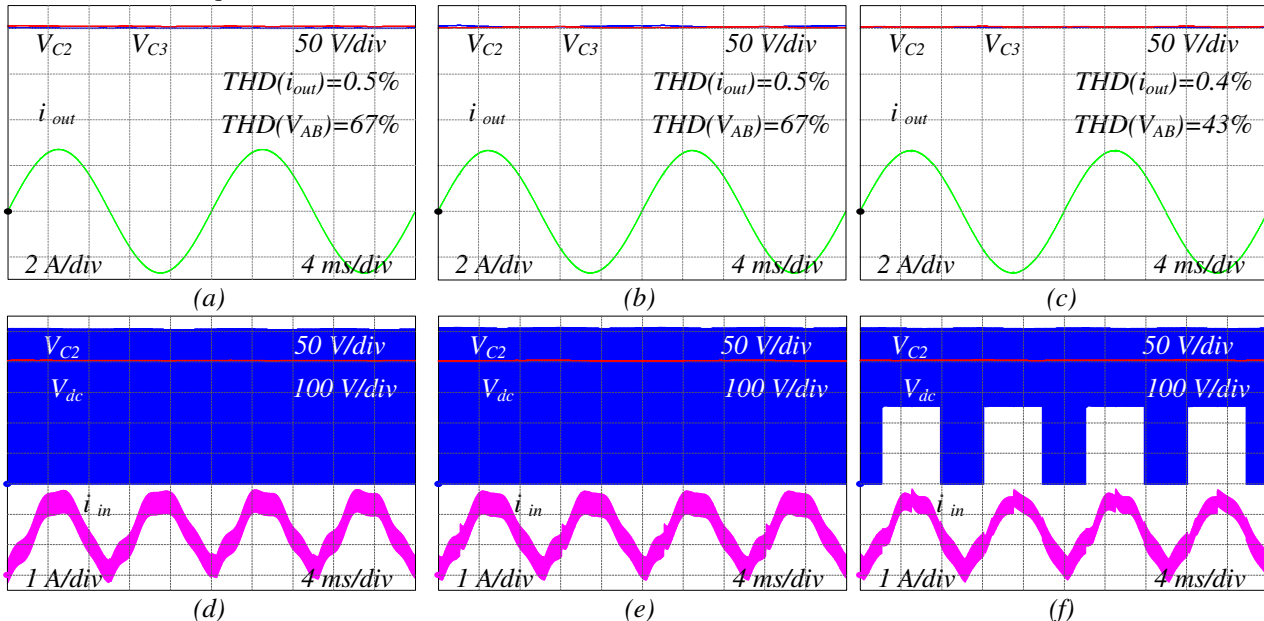

Fig. 11. Simulation results of SPWM (a), (d) proposed SVPWM modulation technique (b), (e) and modified SVPWM (c), (f).

As a result, the control system described above can provide the proposed SVPWM with very high switching frequency and good resolution. At the same time, this control board contains a low cost FPGA and MC that makes it economically viable. In this particular case the switching frequency was reconfigured from 120 kHz till 240 kHz while data exchange frequency was constant 15 kHz.

The modulation technique described above [49] was selected as a reference for our comparison. Fig. 11 shows the simulation waveforms. The input voltage is equal to 300 V with D_S=0.2, output power is about 400 W. The average voltage across capacitors is 400V while the RMS value of output voltage is 230 V. It corresponds to the modulation index M=0.8. Simple resistor is used as a load. Fig. 11a,d illustrate the simulation results with the reference SPWM. At the same time, Fig. 11b,f show the results demonstrated with the proposed SVPWM. Finally, Fig. 11c,g show the proposed modified SVPWM. The dc-link voltage shape V_{dc} of the modified SVPWM differs from other modulations. Incomplete ST states correspond to the half of dc-link voltage.

It can be seen that, all the methods provide a stable voltage across the capacitors and Total Harmonic Distortion (THD) of the output current is very close. At the same time in case of modified SVPWM technique the THD of the output voltage before filter is lower which in turns provides lower THD of the output current. Modified solution has 43% compare to 67% in SVPWM and PWM approaches. It is explained by reduced amount of zero states in dc-ink voltage.

Fig. 12 shows experimental results for SPWM and both SVPWM techniques for fundamental cycle. It shows the dc-link voltage waveform, capacitor voltage along with input current waveforms. First of all this figure shows ability to work at very high switching frequency (240 kHz). Peak value of the input current is about 3 A,

average value twice lower. Despite the very high switching frequency noise presence it can be seen that experimental results are in good correspondence with the simulation results. In case of modified SVPWM (Fig. 12c) the dc-link voltage is different due to the presence of incomplete ST states.

Fig. 13 shows experimental results for only modified SVPWM technique for fundamental (Fig. 13a) and switching cycles (Fig. 13b and Fig. 13c) with the same load condition (400 W). The output current along with capacitor voltage is shown in Fig. 13a. It shows that output current waveform is sinusoidal and is with good agreement with simulation results. Incomplete ST states are utilized and provides transient between neighbor states with minimum transistor switching. Fig. 13b shows the switching cycle when incomplete and full ST states are implemented, while only incomplete ST states generation is demonstrated in Fig. 13c. The input current for switching cycles is demonstrated as well. Because of very high switching frequency the ripple of the input current is very small.

To demonstrate difference between techniques, the number of switching transients (times) in one switching cycle (defined at 50 Hz) was analyzed. These numbers are related to the switching losses represented in Fig. 14 for each modulation technique (D_s is larger than 0). From [49] it is clear that to provide the same ST switching frequency, the carrier signal of the proposed SVPWMs must have the double switching frequency.

Even at double frequency, in the proposed modified SVPWM, the switching states are much more reduced than in the special carrier-based SPWM. At the same time, the overall switching numbers in the proposed SVPWM are approximately the same as in the special carrier-based PWM. The advantage of the SVPWM over the SPWM is in the switching stress between the transistors that are more equally distributed.
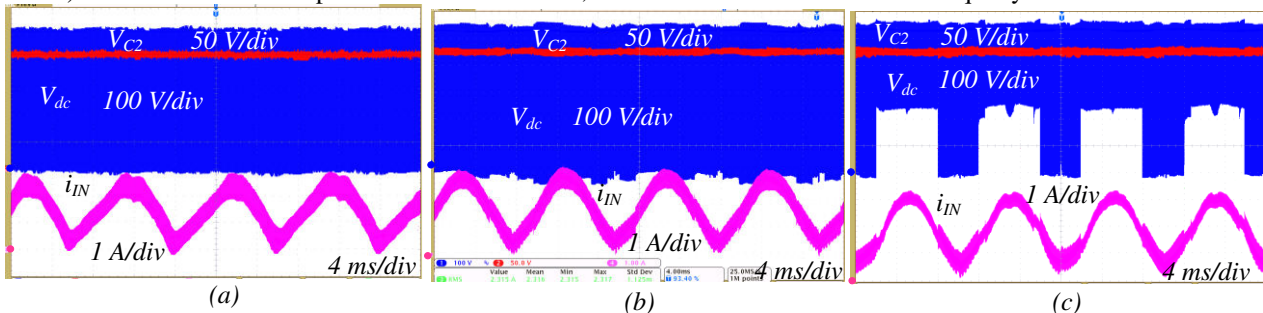

Fig. 12. Experimental results with dc-link voltage, capacitor voltage and input current: SPWM (a), SVPWM (b and modified SVPWM (c).
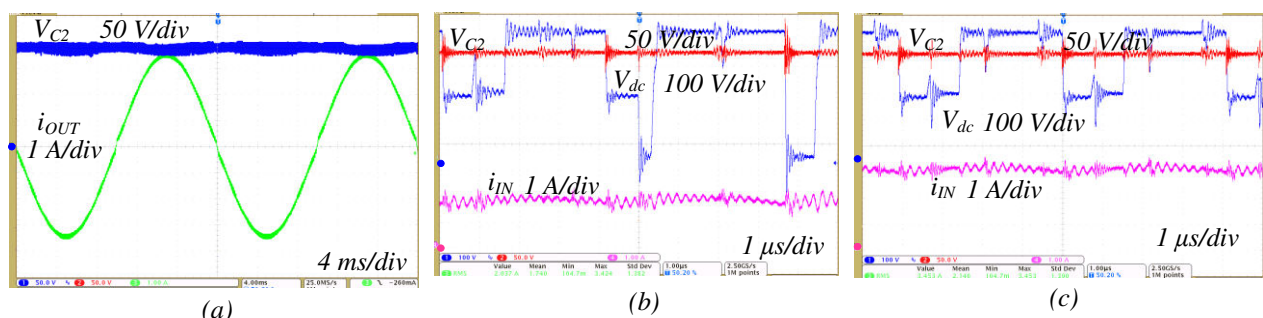

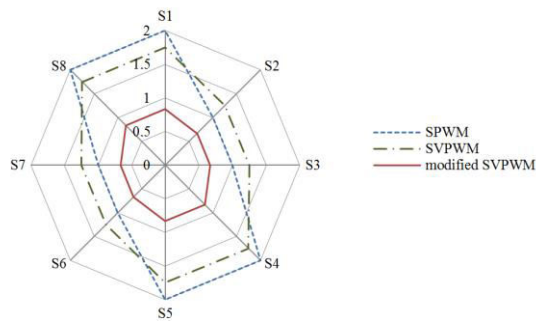Fig. 13. Experimental results of modified SVPWM: fundamental cycle (a), switching cycle (b) and (c).

Fig. 14. Number of switching transients in one switching cycle. SPWM modulation technique versus the proposed SVPWM techniques.

In conclusion, it can be predicted that the modified SVPWM will have lower switching losses. In order to verify this prediction, several tests with different switching frequencies and level of power are performed. Fig. 15a shows the efficiency dependence versus the switching frequency while Fig. 15b shows the efficiency dependence versus the output power with the same input voltage (300 V) and constant ST duty cycle D_s=0.2.
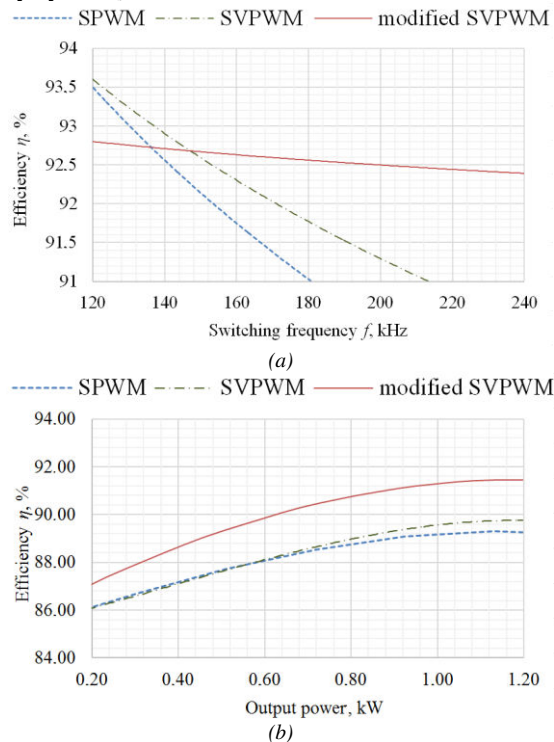

(a)

(b)

Fig. 15.Experimental efficiency versus switching frequency for the different SVPWM techniques for a single-phase IS inverter (a) and efficiency versus output power with switching frequency 240 kHz (b).

It can be seen that the efficiency in the case of the SPWM is significantly reduced by increasing the switching frequency. A similar effect can be observed for the SVPWM and the modified SVPWM. At the same time, it can be seen that the level of incline is different. It means that the level of switching losses in the case of both SVPWMs is lower, in particular in the case of the modified solution. Also, it is evident that in the modified SVPWM, conduction losses are higher. As a result, the overall efficiency is lower at relatively low switching frequency, and significantly better at high switching frequency.

Similar effect can be observed with power increasing. There is some optimal point with the best efficiency, further power increasing will lead to efficiency decreasing.

VI. CONCLUSIONS

This paper has presented novel SVPWM strategies for the single-phase 3L buck-boost full-bridge NPC inverter coupled with IS network. The proposed approach has a minimum number of switching and, as a result, the improved performance is demonstrated in terms of switching losses reduction. The output voltage quality is not worse compared with the traditional PWM strategies. Finally, the switching losses are equally distributed among transistors. Also, the proposed solutions have balanced utilization of all capacitors of the IS network which remains voltage across capacitors stable.

It should be noticed, that as any SVM technique, more complex calculation compare to the PWM is required. The main drawback of the proposed technique consists in the increased conduction losses due to the utilizing only single leg of the full-bridge NPC converter during ST generation. It belongs mostly to the MOSFET transistors, where losses are proportional to the drain-source resistance. Because of that, such approach can be recommended for inverters realized by MOSFET transistor with very high switching frequency, where switching losses dominates over conduction losses. Another application can be based on IGBT transistors, where switching losses decreasing will allow increasing switching frequency.

Theoretical claims are verified by means of simulation and experimental study.

ACKNOWLEDGMENT

VII. REFERENCES

[1] Representing the global wind energy industry. (2016). [ebook] Global Wind Energy Council. Available at: http://www.gwec.net/wp-content/uploads/vip/GWEC-PRstats-2015_LR.pdf [Accessed 10 Apr. 2016].

[2] www.vestas.com, V. (2016). *Vestas | Turbines*. [online] Vestas.com. Available at: https://www.vestas.com/en/products/turbines# [Accessed 10 Apr. 2016].

[3] G. K. Dey, K.T. Ahmmed, "Multi-junction solar cells and microwave power transmission technologies for solar power satellite" *In Proc. Informatics, Electronics & Vision (ICIEV), 2014 International Conference on.*, pp. 1-6, 2014.

[4] G. F. X Strobl, L. Ebel, D. Fuhrmann, W. Guter, R. Kern, V. Khorenko, M. Meusel, "Development of lightweight space solar cells with 30% efficiency at end-of-life" *In Proc. Photovoltaic Specialist Conference (PVSC)*, pp. 3595-3600, 2014.

[5] F.Z. Peng, "Z-Source Inverter," *IEEE Trans. Ind. Applicat.*, vol. 39, no. 2, pp. 504-510, Mar./Apr. 2003.

[6] A. Chub, O. Husev, J. Zakis and J. Rabkowski, "Switched-capacitor current-fed quasi-Z-source inverter", *In Proc. 14th Biennial Baltic Electronic Conference (BEC),* pp. 229-232, Tallinn, 2014.

[7] Y.P. Siwakoti, F. Peng, F. Blaabjerg, P.C. Loh, G.E. Town, "Impedance Source Networks for Electric Power Conversion Part-I: A Topological Review," *IEEE Trans. Power Electron.*, vol.30, no. 2, pp. 699-716, Feb. 2015.

[8] O. Husev, L. Liivik, F. Blaabjerg, A. Chub, D. Vinnikov, I. Roasto. "Galvanically Isolated Quasi-Z-Source DC-DC Converter with a Novel ZVS and ZCS Technique", *IEEE Trans. Ind. Electron.*, vol 62, no 12, pp. 7547-7556, 2015.

[9] A. Chub, D. Vinnikov, F. Blaabjerg, F.Z. Peng "A Review of Galvanically Isolated Impedance-Source DC–DC Converters" *IEEE Trans. Power Electron.*, vol. 31, no. 4, pp. 2808 - 2828, April 2016.

[10] Y.P. Siwakoti, F. Peng, F. Blaabjerg, P. Loh, G.E. Town, "Impedance Source Networks for Electric Power Conversion Part-II: Review of Control Method and Modulation Techniques," *IEEE Trans. Power Electron.*, vol.30, no. 4, pp. 1887 - 1906, April 2015.

[11] T. Shults, O. Husev O. J. Zakis, "Overview of impedance source networks for voltage source inverters", *In Proc. Micro/Nanotechnologies and Electron Devices (EDM), 2015 16th International Conference of Young Specialists on*., pp. 514-520, 2015.

[12] L. G Franquelo, J. Rodriguez, J. I. Leon, S. Kouro, R. Portillo, M. A. M. Prats, "The age of multilevel converters arrives", *IEEE Ind. Electron. Mag*., vol. 2, no. 2, pp. 28–39, Jun. 2008.

[13] J. Rodríguez, J. S. Lai, F. Z. Peng, "Multilevel Inverters: A Survey of topologies, controls, and applications", *IEEE Trans. Ind. Electron.,* vol. 49, no. 4, pp.724-738, August 2002.

[14] S. Tenner, S.Tenner, W. Hofmann, "A comparison of Z-Source three-level NPC inverter versus Z-Source two-level inverter." *In Emobility-Electrical Power Train*, pp. 1-7. IEEE, 2010.

[15] O. Husev, C. Roncero-Clemente, E. Romero-Cadaval, D. Vinnikov, S. Stepenko, "Single phase three-level neutral-point-clamped quasi-Z-source inverter ", *IET Power Electron*., vol. 8, no. 1, pp. 1-10, 2015.

[16] Y. Liu, B. Ge, H. Abu-Rub, D. Sun, "Comprehensive modeling of single-phase quasi-Z-source photovoltaic inverter to investigate low-frequency voltage and current ripple," *IEEE Trans. Ind. Electron.*, vol. 67, pp. 4194-4202, 2015.

[17] S. Kouro, M. Malinowski, K Gopakumar, J. Pou, L. G Franquelo, B. Wu, J. Rodriguez, M. A. Perez, J. I. Leon, "Recent advances and industrial applications of multilevel converters," *IEEE Trans. Ind. Electron*., vol.57, no.8, pp.2553-2580, Aug. 2010.

[18] M. Dybko, S. Brovanov, S. Kharitonov, "Mathematical simulation technique for power systems based on diode-clamped multilevel VSC", in Proc. of EuroCon 2013, Zagreb, pp. 941–947, 1–4 July 2013.

[19] D. Panfilov, O. Husev, F. Blaabjerg, J. Zakis, K. Khandakji, "Comparison of three-phase three-level voltage source inverter with intermediate dc–dc boost converter and quasi-Z-source inverter", *IET Power Electron.*, vol. 9, no. 6, pp. 1238-1248, 2016.

[20] R. Burkart, J. W. Kolar, G. Griepentrog „Comprehensive comparative evaluation of single- and multi-stage three-phase power converters for photovoltaic applications," *in Proc. of Intelec, 2012*, pp. 1-8.

[21] O. Husev, F. Blaabjerg, C. Roncero-Clemente, E. Romero-Cadaval, D. Vinnikov, Y. P. Siwakoti, R. Strzelecki, "Comparison of Impedance-Source Networks for Two and Multilevel Buck-Boost Inverter Applications", *IEEE Trans. Power Electron.,* vol. 31, no. 11, pp. 7564-7579, Nov. 2016.

[22] F. Z. Peng, M. Shen, and Z. Qian, "Maximum boost control of the Z-source inverter". *IEEE Trans. Power Electron*, Vol. 20, No. 4, pp. 833–838, July 2005.

[23] P. C. Loh, F. Gao, F. Blaabjerg, S. Yun, C. Feng, K. N. J. Soon "Pulse width-Modulated Z-Source Neutral-Point-Clamped Inverter". *IEEE Trans. Ind. Applicat,* vol.43, no.5, pp.1295-1308, Sept.-Oct. 2007.

[24] P. C. Loh, F. Blaabjerg and C. P. Wong, "Comparative Evaluation of Pulse-width Modulation Strategies for Z-Source Neutral-Point-Clamped Inverter", *IEEE Trans. Power Electron*., vol. 22, no. 3, pp. 1005-1013, May 2007.

[25] P. C. Loh, F. Gao, F. Blaabjerg, "Topological and Modulation Design of Three-Level Z-Source Inverters". *IEEE Trans. Power Electron*, vol. 23, no. 5, pp. 2268-2277, Sep. 2008.

[26] J. H. G. Muniz, E.R.C. da Silva and E.C. dos Santos Jr., "A Hybrid PWM Strategy for Z-Source Neutral-Point-Clamped inverter", in Proc. IEEE APEC 2011, pp. 450-456, Mar. 2011.

[27] O. Husev, C. Roncero-Clemente, E. Romero-Cadaval, D. Vinnikov, T. Jalakas, "Three-level three-phase quasi-Z-source neutral-point-clamped inverter with novel modulation technique for photovoltaic application", *Electric Power Systems Research,* vol. 130, no. 1, pp. 10–21, 2016.

[28] Y. Liu, B. Ge, H. Abu-Rub, F. Z. Peng, "Phase-shifted pulse-width-amplitude modulation for quasi-Z-source cascade multilevel inverter-based photovoltaic power system," *IET Power Electron.*, vol.7, no. 6, pp.1444-1456, 2014.

[29] P. C. Loh, F. Gao, F. Blaabjerg and S. W. Lim, "Operational Analysis and Modulation Control of Three-Level Z-Source Inverters With Enhanced Output Waveform Quality," *IEEE Trans. Power Electron*., vol. 24, no. 7, pp. 1767-1775, July 2009.

[30] F. Gao, P. C. Loh, F. Blaabjerg and R. Teodorescu, "Modulation Schemes of Multi-Phase Three Level Z-Source Inverters," *in Proc. of PESC 2007*, pp. 1905-1911, June 2007.

[31] O. Ellabban, J. Van Mierlo, P. Lataire, "Comparison between different PWM control methods for different Z-source inverter topologies", *in Proc. of 13th IEE European Conference on Power Electronics and Applications, EPE '09*, pp.1-11, 8-10 Sept. 2009.

[32] Y. Liu, B. Ge, F. J. T. E. Ferreira, A. T. de Almeida and H. Abu-Rub, "Modelling and SVM Control of quasi Z-Source Inverter". *In Proc. 11th International Conference in Electr. Power Quality Utilization*, pp.1-7, Oct. 2011.

[33] U. S. Ali and V. Kamaraj, "A novel space vector PWM for Z-source inverter". *In Proc. 1st International Conference on Electrical Energy Systems (ICEES), Newport Beach, CA,* pp. 82-85. 2011.

[34] Y. Liu, B. Ge, H. Abu-Rub and F. Z. Peng, "Overview of Space Vector Modulations for Three-Phase Z-Source/Quasi-Z-Source Inverters", *IEEE Trans. Power Electron*., vol. 29, no. 4, pp. 2098-2108, April 2014.

[35] Y. Liu, B. Ge and H. Abu-Rub, "Theoretical and experimental evaluation of four space vector modulations applied to quasi-z-source inverters". *IET Power Electron,* vol. 6, no. 7, pp. 1257-1269, August 2013.

[36] Y. P. Siwakoti and G. E. Town, "Three-phase transformerless grid connected Quasi Z-Source Inverter for solar photovoltaic systems with minimal leakage current", *In Proc. 3rd IEEE International Symposium on Power Electronics for Distributed Generation Systems (PEDG)*, pp. 368-373. Aalborg, 2012.

[37] F. Bradaschia, M. C. Cavalcanti, P. E. P. Ferraz, F. A. S. Neves, E. C. dos Santos and J. H. G. M. da Silva, "Modulation for Three-Phase Transformerless Z-Source Inverter to Reduce Leakage Currents in Photovoltaic Systems", *IEEE Trans. Ind. Electron*., vol. 58, no. 12, pp. 5385-5395, Dec. 2011.

[38] P. Majtczak, J. Rabkowski, "Symmetrical Switching Patterns and an Adaptive Modulator for Three-Phase Quasi-Z-Source Inverters", 2017 IEEE 26th International Symposium on Industrial Electronics (ISIE), pp. 1676 – 1681.

[39] Y. P. Siwakoti and G. E. Town, "Common-mode voltage reduction techniques of three-phase Quasi Z-Source Inverter for AC drives", *In Proc. Twenty-Eighth Annual IEEE Applied Power Electronics Conference and Exposition (APEC)*, pp. 2247-2252. Long Beach, CA, 2013.

[40] F.B. Effah, P. Wheeler, J. Clare, A. Watson, "Space-Vector-Modulated Three-Level Inverters With a Single Z-Source Network". *IEEE Trans. Power Electron*., vol.28, no.6, pp.2806-2815, June 2013.

[41] Y. Liu, G. Baoming, H. Abu-Rub, F. Z. Peng, "A Modular Multilevel Space Vector Modulation for Photovoltaic Quasi-Z-Source Cascaded Multilevel Inverter,", *in Proc. of IEEE APEC 2013*, pp. 714-18, Mar. 2013.

[42] X. You, S. Liu, H. Abu-Rub; B. Ge, X. Jiang; F. Z. Peng, "A new space vector modulation strategy to reduce common-mode voltage for quasi-Z-source indirect matrix converter", in Proc. of Energy Conversion Congress and Exposition (ECCE), 2014 IEEE. – IEEE, 2014. 1064-1069.

[43] A. A. Abduallah, A. Iqbal, L. Ben-Brahim, "Space vector pulse width modulation techniques for a five-phase impedance source and quasi impedance source inverters", *in Proc. IEEE International Conference on Industrial Technology (ICIT)*, pp. 1173-1178, 2015.

[44] Z. Zhang, Y.X. Xie, W.P. Huang, J.Y. Le, and L. Chen, "A new SVPWM method for single-phase three-level NPC inverter and the control

method of neutral point voltage balance," in Proc. of *International Conference on Electrical Machines and Systems, 2009. ICEMS 2009*, pp. 1-4. IEEE, 2009.

[45] R.T Shreiner. "Vektornye sistemy shirotno-impul'snoi modulyatsii," Matematicheskoe modelirovanie elektroprivodov peremennogo toka s poluprovodnikovymi preobrazovatelyami chastoty, Ekaterinburg, Russia: UrO RAN, 2000, pp. 405-420 (in Russian).

[46] S.V. Brovanov, S.A. Kharitonov, M.A. Dybko, E.V. Grishanov, "A new approach for current calculation in a single-phase three-level NPC converter with space vector PWM," *in Proc. of IEEE Region 8 International Conference on Computational Technologies in Electrical and Electronics Engineering, SIBIRCON 2010*, pp. 639–644.

[47] J. Guzman-Guemez, D.S. Laila, S.M. Sharkh, "State-space approach for modelling and control of a single-phase three-level NPC inverter with SVPWM," *In Proc. of Power and Energy Society General Meeting (PESGM)*, 2016, pp. 1-5. IEEE, 2016.

[48] T. Shults, O. Husev, F. Blaabjerg, "Design of Three-Phase Three-Level CIC T-Source Inverter with Maximum Boost Control in *Proc. of IEEE-IECON*, 2015, pp. 2408-2413.

[49] C. Roncero-Clemente, O. Husev, T. Jalakas, E. Romero-Cadaval, J. Zakis, V. Mmiñambres-Marcos, "PWM for Single Phase 3L Z/qZ Source Inverter with Balanced Power Losses". *Elektronika ir Elektrotechnika*, vol. 20, no. 6, pp. 71-76, 2014.

Tatiana E. Shults received the B.Sc., M.Sc. degrees in industrial electronics and PhD professional skill "Researcher. Lecture-researcher" from Novosibirsk State Technical University, Novosibirsk, Russia in 2012, 2014 and 2018 respectively.

She is engineer of 2nd category of the Power Electronics Institute of Novosibirsk State Technical University. In 2015 she had semiannual internship in the Power Electronics Group, Department of Electrical Power Engineering and Mechatronics, Tallinn University of Technology (Estonia).

Her research interests are in power electronics systems: application of photovoltaic panels as power sources in generation systems; dc-ac multilevel converters; design of power converters and control systems, impedance source inverters. She has over 13 publications
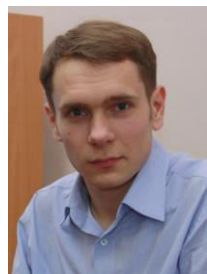
Oleksandr Husev (S'10–M'12) received the B.Sc. and M.Sc. degrees in industrial electronics from Chernihiv State Technological University, Chernihiv, Ukraine, in 2007 and 2008 respectively. He defended PhD thesis in the Institute of Electrodynamics of the National Academy of Science of Ukraine in 2012.

He is senior researcher of the Department of Electrical Power Engineering and Mechatronics, Tallinn University of Technology and associate professor of the Department of Biomedical Radioelectronics Apparatus and Systems, Chernihiv National University of Technology. He has over 60 publications and is the holder of several patents.

His research interests are in Power Electronics systems. Design of novel topologies, control systems based on a wide range of algorithms, including modeling, design, and simulation. Applied design of power converters and control systems and application, stability investigation.

Frede Blaabjerg (S'86–M'88–SM'97–F'03) was with ABB-Scandia, Randers, Denmark, from 1987 to 1988. From 1988 to 1992, he got the PhD degree in Electrical Engineering at Aalborg University in 1995. He became an Assistant Professor in 1992, an Associate Professor in 1996, and a Full Professor of power electronics and drives in 1998. From 2017 he became a Villum Investigator. He is honoris causa at University Politehnica Timisoara (UPT), Romania and Tallinn Technical University (TTU) in Estonia. His current research interests include power electronics and its applications such as in wind turbines, PV

systems, reliability, harmonics and adjustable speed drives. He has published more than 500 journal papers in the fields of power electronics and its applications. He is the co-author of two monographs and editor of 7 books in power electronics and its applications.

He has received 26 IEEE Prize Paper Awards, the IEEE PELS Distinguished Service Award in 2009, the EPE-PEMC Council Award in 2010, the IEEE William E. Newell Power Electronics Award 2014 and the Villum Kann Rasmussen Research Award 2014. He was the Editor-in-Chief of the IEEE TRANSACTIONS ON POWER ELECTRONICS from 2006 to 2012. He has been Distinguished Lecturer for the IEEE Power Electronics Society from 2005 to 2007 and for the IEEE Industry Applications Society from 2010 to 2011 as well as 2017 to 2018. In 2018 he is President Elect of IEEE Power Electronics Society.

He is nominated in 2014, 2015, 2016 and 2017 by Thomson Reuters to be between the most 250 cited researchers in Engineering in the world.

Carlos Roncero-Clemente (S'11–M'16) was born in Badajoz, Spain, in 1984. He received the B.Sc. degree in electrical engineering with honors, the M.Sc. degree in industrial engineering with honors, the M.Sc. degree in engineering and architecture research, and the Ph.D. degree in industrial engineering from the University of Extremadura, Badajoz, Spain, in 2006, 2008, 2011, and 2016, respectively. During his Ph.D. research, he was a Visiting Student at Tallinn University of Technology, Tallinn, Estonia, and at Aalborg University, Aalborg, Denmark. He is currently a Postdoctoral Researcher with Nova University of Lisbon, Lisbon, Portugal and member of PE&ES Research Group at University of Extremadura. His research interests include power electronic interfaces, modulation techniques, modeling and simulations, renewable energy sources, and smart grids.

Enrique Romero-Cadaval (S'02–M'05–SM'10) received the M.Sc. degree in industrial electronic engineering from the Escuela Técnica Superior de Ingeniería Industrial (ICAI), Universidad Pontificia de Comillas, Madrid, Spain, in 1992, and the Ph.D. degree from the Universidad de Extremadura, Badajoz, Spain, in 2004. In 1995, he joined the University of Extremadura where he teaches power electronics and researches within the Power Electrical and Electronic Systems (PE&ES) R&D Group in the School of Industrial Engineering. His has participated in several projects dealing with power electronics applied to power systems, power quality, active power filters, electric vehicles, smart grids, and renewable energy resources. He is a Senior Member of the IEEE.

Dmitri Vinnikov (M'07–SM'11) received the Dipl.Eng., M.Sc., and Dr.Sc.techn. degrees in electrical engineering from Tallinn University of Technology, Tallinn, Estonia, in 1999, 2001, and 2005, respectively.

He is currently the Head of the Power Electronics Group, Department of Electrical Power Engineering and Mechatronics, Tallinn University of Technology (Estonia) and a Guest Researcher at the Institute of Industrial Electronics and Electrical Engineering, Riga Technical University (Latvia). He is the Head of R&D and co-founder of Ubik Solutions LLC - Estonian start-up company dedicated to innovative & smart power electronics for renewable energy systems. Moreover, he is one of the founders and leading researchers of ZEBE – Estonian Centre of Excellence for zero energy and resource efficient smart buildings and districts. He has authored or coauthored two books, five monographs and one book chapter as well as more than 200 published papers on power converter design and development and is the holder of numerous patents and utility models in this field. His research interests include applied design of power electronic converters and control systems, renewable energy conversion systems (photovoltaic and wind), impedance-source power converters, and implementation of wide bandgap power semiconductors.